Figuring Out a Complicated World

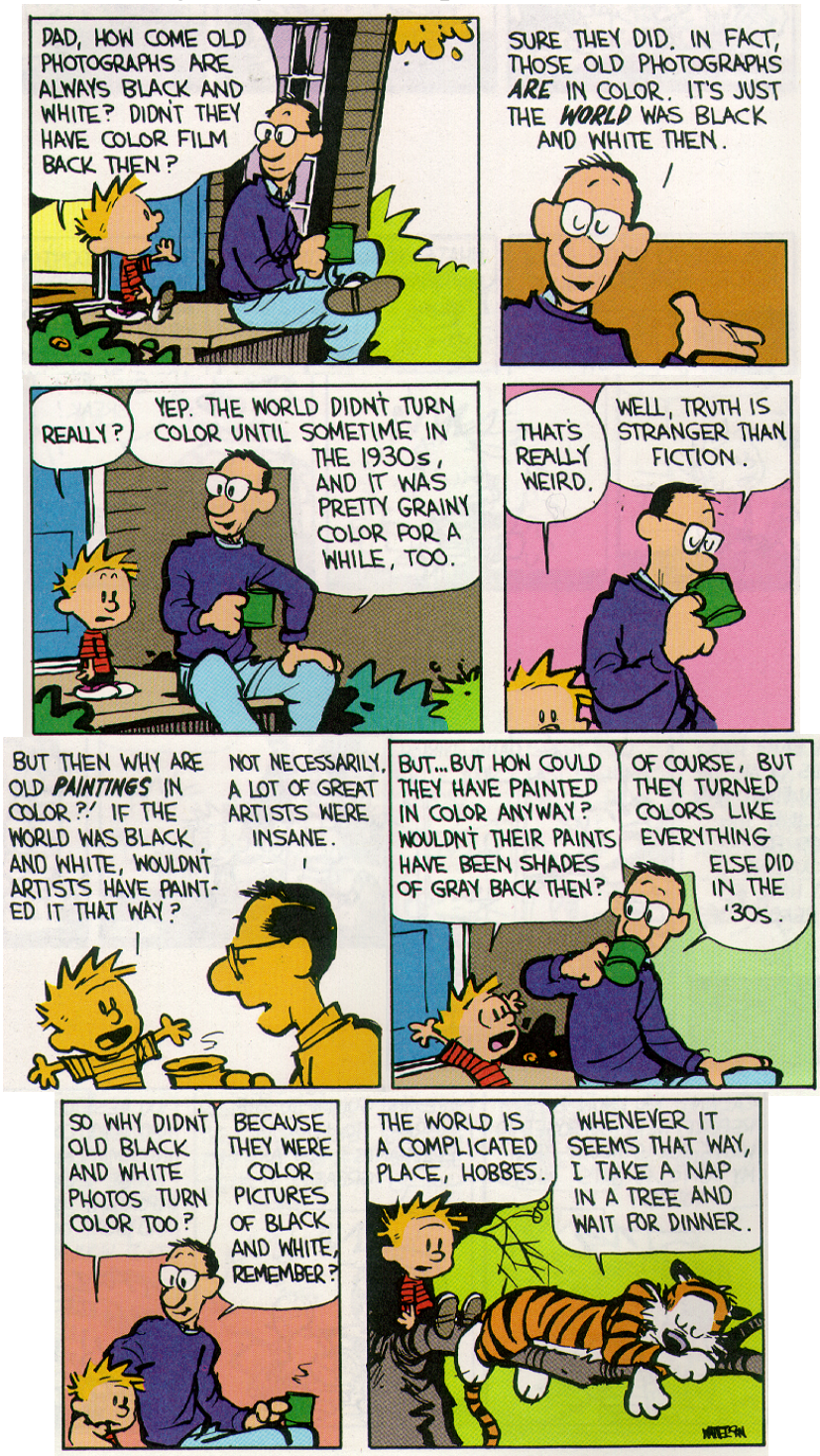

I have felt like taking many naps during the last seven years. Fortunately I didn't.

TABLE OF CONTENTS

Table 2.1. Summary of Flask Sampling Stations in the Scripps O_2/N_2 Network

Station code	Station	Latitude	Longitude	Elevation (m a.s.l.)	Time period
ALT	Alert, Northwest Territories, Canada	82°27'N	62°31'W	210	Nov. 1989 – May 2000
CBA	Cold Bay, Alaska, USA	55°12'N	162°43'W	25	Aug. 1995 – May 2000
NWR	Niwot Ridge, Colorado, USA	40°03'N	105°38'W	3749	Apr. 1991 – Apr. 1993
LJO	La Jolla, California, USA	32°52'N	117°15'W	15	May 1989 – June 2000
MLO	Mauna Loa, Hawaii, USA	19°32'N	155°35'W	3397	Jan. 1991 – May 2000
KUM	Cape Kumukahi, Hawaii, USA	19°31'N	154°49'W	3	June 1993 – May 2000
SMO	Cape Matatula, American Samoa, USA	14°15'S	170°34'W	42/93*	June 1993 – Apr. 2000
CGO	Cape Grim, Tasmania, Australia	40°41'S	144°41'E	94	Jan. 1991 – Dec. 1999
MCQ	Macquarie Island, Australia	54°29'S	158°58'E	94	Sep. 1992 – Jan. 1994
PSA	Palmer Station, Antarctica	64°55'S	64°00'W	10	Sep. 1996 – Mar. 2000
SPO	South Pole Station, Antarctica	89°59'S	24°48'W	2810	Nov. 1991 – Dec 1999

* In May 1999 a new sampling intake was installed on a new tower, 93 m above sea level.

minimum of 15 flask volumes have passed through each flask, then the sample is sealed off, at a pressure of approximately 1 bar. A back pressure regulator is employed at stations located significantly above sea level to achieve 1 bar of pressure in the flasks. A cold trap at temperatures ranging from -55°C to -90°C, depending on the station, pre-dries the air to remove water vapor. Samples are collected in a temperature-controlled environment to minimize possible fractionation effects. Flask samples are shipped back to our laboratory in La Jolla for analysis. In the case of South Pole (SPO) and Macquarie Island, samples may be stored on site for as long as ten months before they are shipped back to La Jolla, and as long as two months at Palmer Station (PSA). All other stations ship samples back within three weeks of collection.

Flask samples are collected by station personnel during what are considered to be "clean, background air" conditions. The general criteria used to determine when these conditions are met is a pre-established wind direction and speed, and where

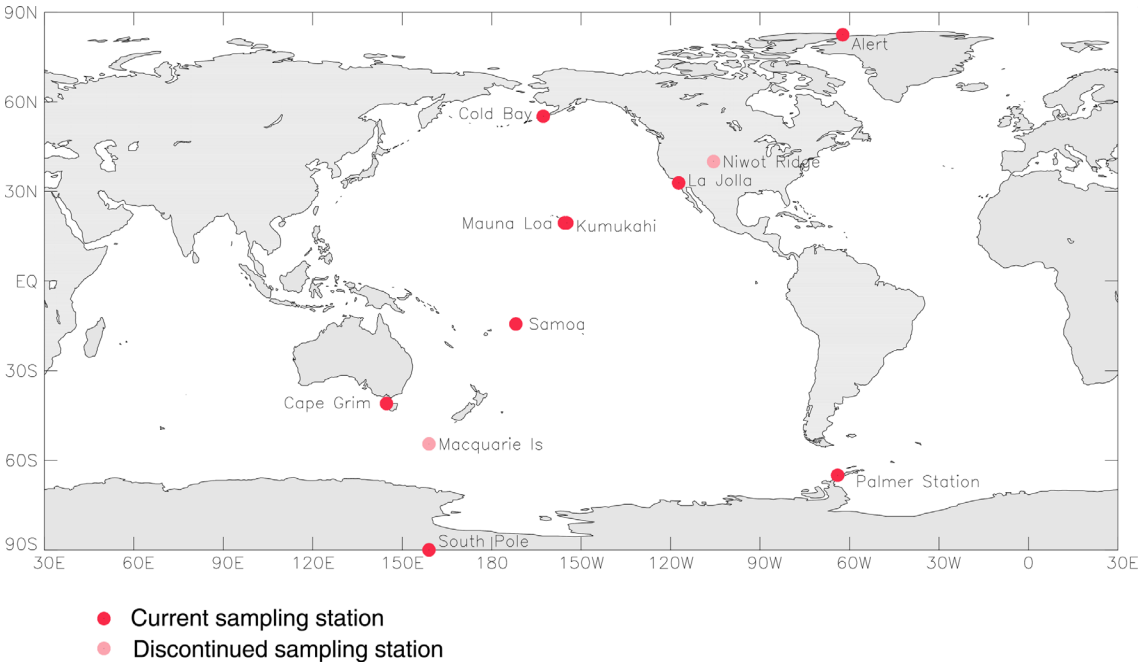

Figure 2.1. Map showing the locations of the eleven sampling stations in the Scripps O_2/N_2 network as listed in Table 2.1. Mauna Loa (MLO) and Cape Kumukahi (KUM) are shown as one point. Niwot Ridge (NWR) and Macquarie Island (MCQ) stations have now been discontinued. With the exceptions of Niwot Ridge (3749 m), Mauna Loa (3397 m) and South Pole (2810 m), all stations are approximately at sea level and coastal and therefore they are situated in the marine boundary layer.

available, relatively steady, non-fluctuating, *in situ* atmospheric CO_2 concentrations, or criteria based on other trace gas species which are measured *in situ*. We wish to sample air that has not been contaminated by local or regional anthropogenic or terrestrial processes.

In this manner we can observe synoptic and hemispheric-scale spatial trends, and seasonal and interannual temporal trends. Thus, for example, stations such as La Jolla (LJO) and Cape Grim (CGO), require a relatively narrow wind direction window (roughly westerlies for both stations) to meet these sampling requirements. Cape

summer gas solubilites decrease driving a flux of O_2 and N_2 into the atmosphere. The N_2 solubility dependence on temperature is less than that of O_2 resulting in an increase in the O_2/N_2 ratio. During fall and winter surface waters cool, gas solubilities increase, and more O_2 re-dissolves than N_2, decreasing the atmospheric O_2/N_2 ratio. The remaining 85% or so of the APO seasonal cycle is due to ocean biota. During fall and winter the mixed layer deepens as surface waters cool, become more dense and sink, entraining water that is undersaturated in O_2. At the same time there is less net photosynthesis because of less solar irradiance and because the mixed layer is deeper than the euphotic zone, so phytoplankton spend less time in a region with available energy for photosynthesizing. These processes all combine to create a net atmospheric O_2 demand. In the spring and summer the mixed layer shoals, concentrating phytoplankton in the surface waters which receive the most sunlight, there is more net solar irradiance, and temperatures are warmer, all combining to result in higher net photosynthesis. Additionally, because of the shallow mixed layer, O_2 is concentrated in the surface waters. All of these processes result in O_2-supersaturated surface waters and a flux of O_2 to the atmosphere.

Figures 2.6, 2.7, and 2.8 show respectively the O_2/N_2, CO_2, and APO harmonic curve fits for all stations superimposed on each other for comparison. Cold Bay exhibits the largest amplitude in O_2/N_2 ratio and in APO (Table 2.2), with O_2/N_2 ratio over 20 per meg higher than the next highest, Alert, and APO almost 30 per meg higher than the next highest in the northern hemisphere. I suspect that this large amplitude is owing to the proximity of Cold Bay to regions of highly active air-sea exchange of O_2 in the North Pacific and Bering Sea. This conclusion is further supported by data from an

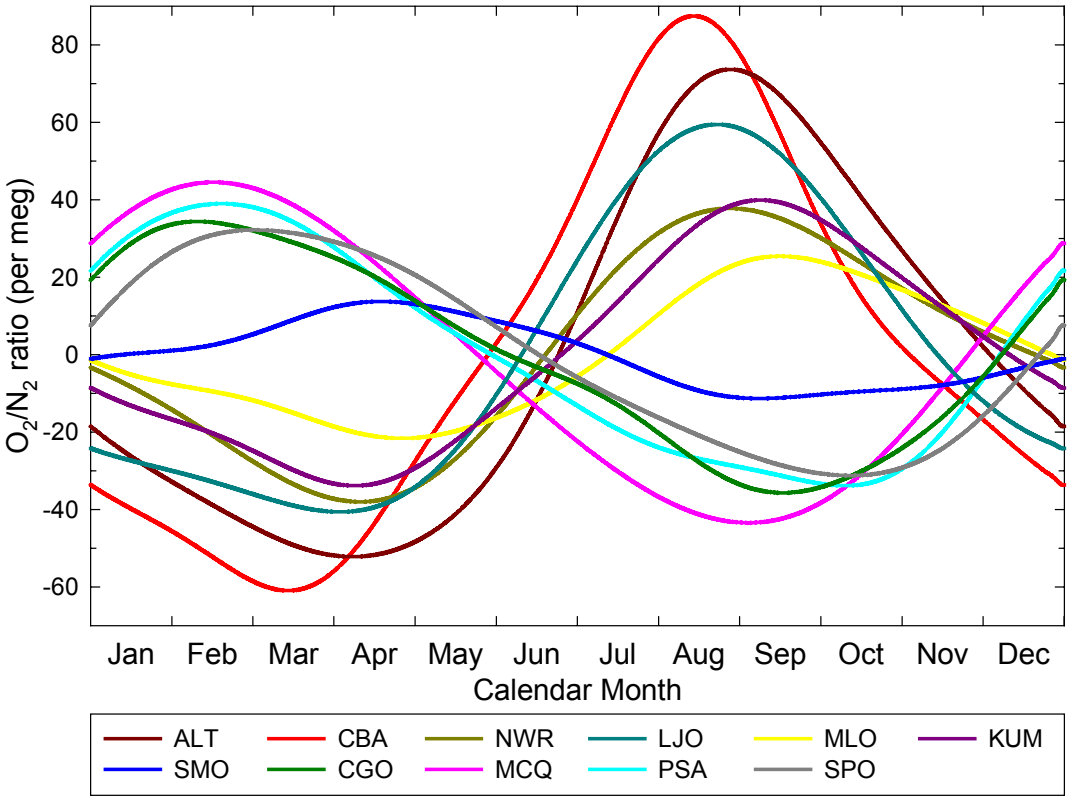

Figure 2.6. Shows the seasonal cycle component of the curve fits from Figure 2.2 for O_2/N_2 ratios for all stations, after correcting data as described in Section 2.2.3. Amplitude and phasing variations can be compared between different stations in this figure.

independent O_2/N_2 sampling program at Point Barrow, Alaska (71°19'N, 156°36'W), also in close proximity to the Bering Sea, where similar large seasonal amplitudes are observed (M. Bender, personal communication).

Cold Bay also shows a significantly earlier minimum in both O_2/N_2 ratios and APO and a slightly earlier maximum in CO_2 than other northern hemisphere stations (Figures 2.6, 2.7, and 2.8), indicating an earlier start of the "spring thaw" in both the marine and land biota. Alert exhibits the latest start in the spring thaw, as could be

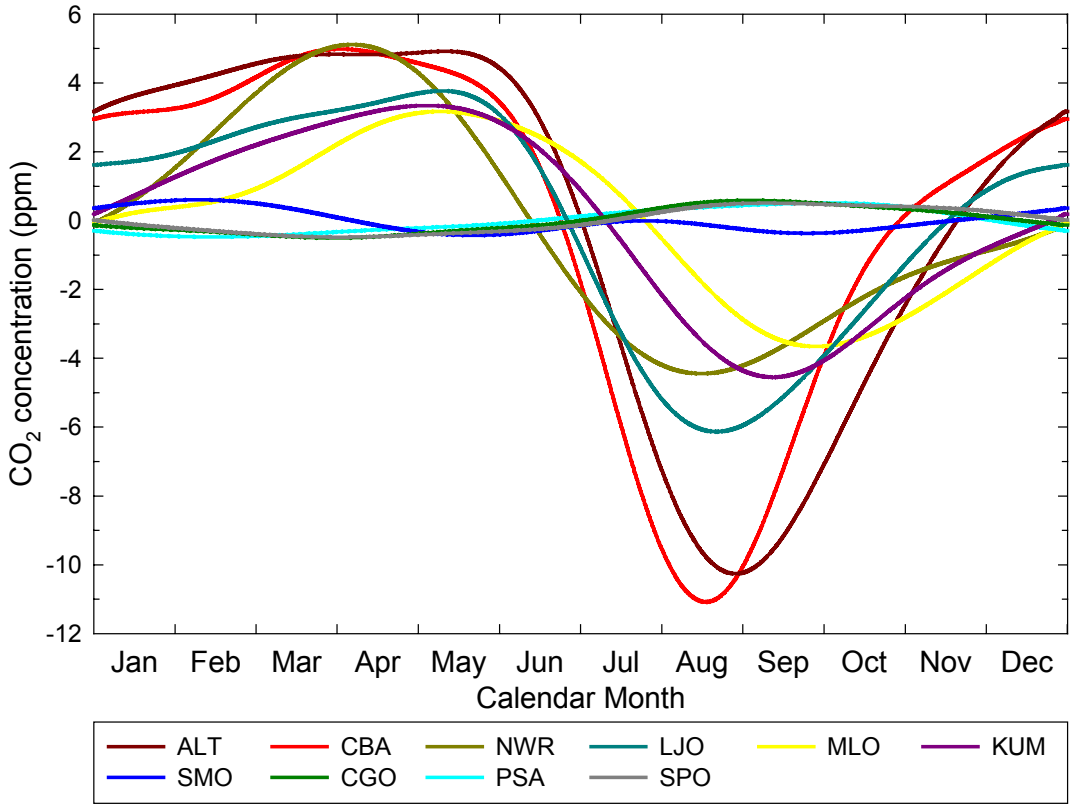

Figure 2.7. Shows the seasonal cycle component of the curve fits from Figure 2.3 for CO_2 concentration for all stations, after correcting data as described in Section 2.2.3.

expected by a high northern latitude station. The same reason given for Cold Bay exhibiting the largest amplitude, the proximity to sources and sinks, can also explain the significantly earlier spring rise and fall decrease in O_2/N_2 ratios. The Cold Bay APO signal shows greater asymmetry compared to other stations, particularly noticeable in the spring. This I attribute to the marine and land biota being slightly out of phase in this region in terms of the start of the spring thaw.

The seasonal APO cycles at Niwot Ridge and Mauna Loa are the smallest observed because both of these sites are situated at elevations that place them above the

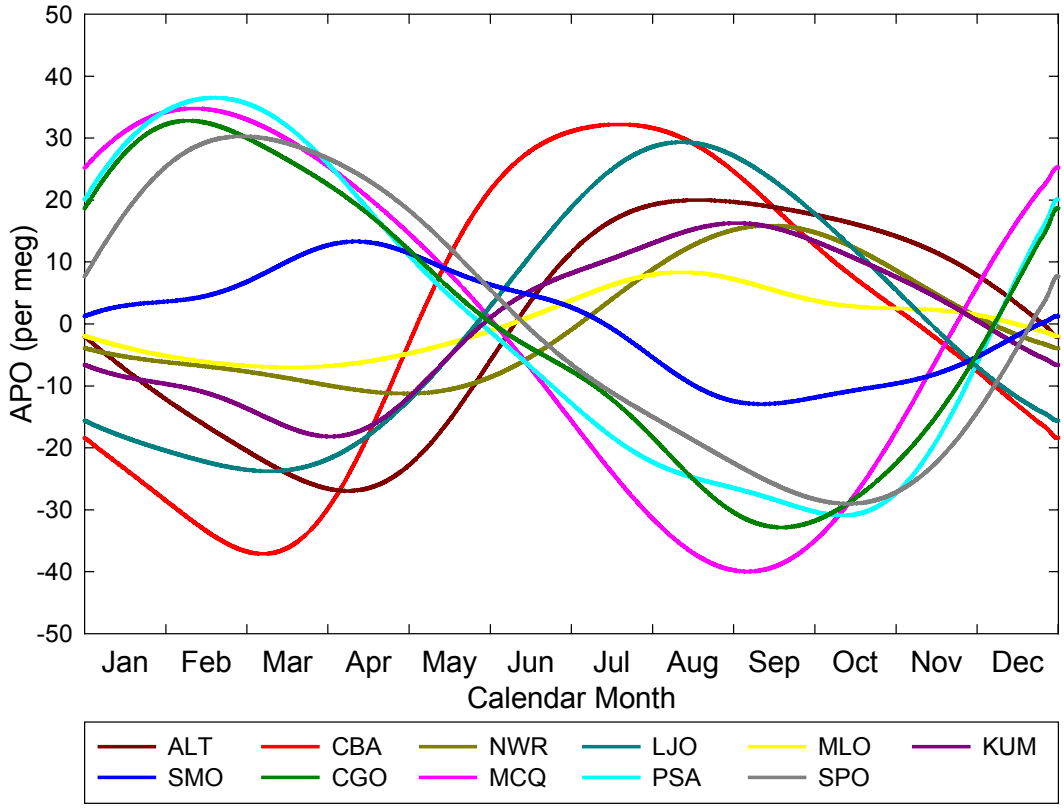

Figure 2.8. Shows the seasonal cycle component of the curve fits from Figure 2.4 for APO for all stations, after correcting data as described in Section 2.2.3.

marine boundary layer, and the surface-based ocean fluxes driving the seasonal cycles are attenuated at these altitudes. South Pole is also at higher elevation and shows some attenuation in APO compared to other mid- to high latitude southern hemisphere stations. The reason why South Pole does not exhibit the same attenuation as observed at Mauna Loa and Niwot Ridge is probably because it is surrounded by regions of active air-sea gas exchange.

The smallest seasonal cycles are observed in the tropical stations of Mauna Loa, Cape Kumukahi, and Samoa, as expected due to the low seasonality in these locations.

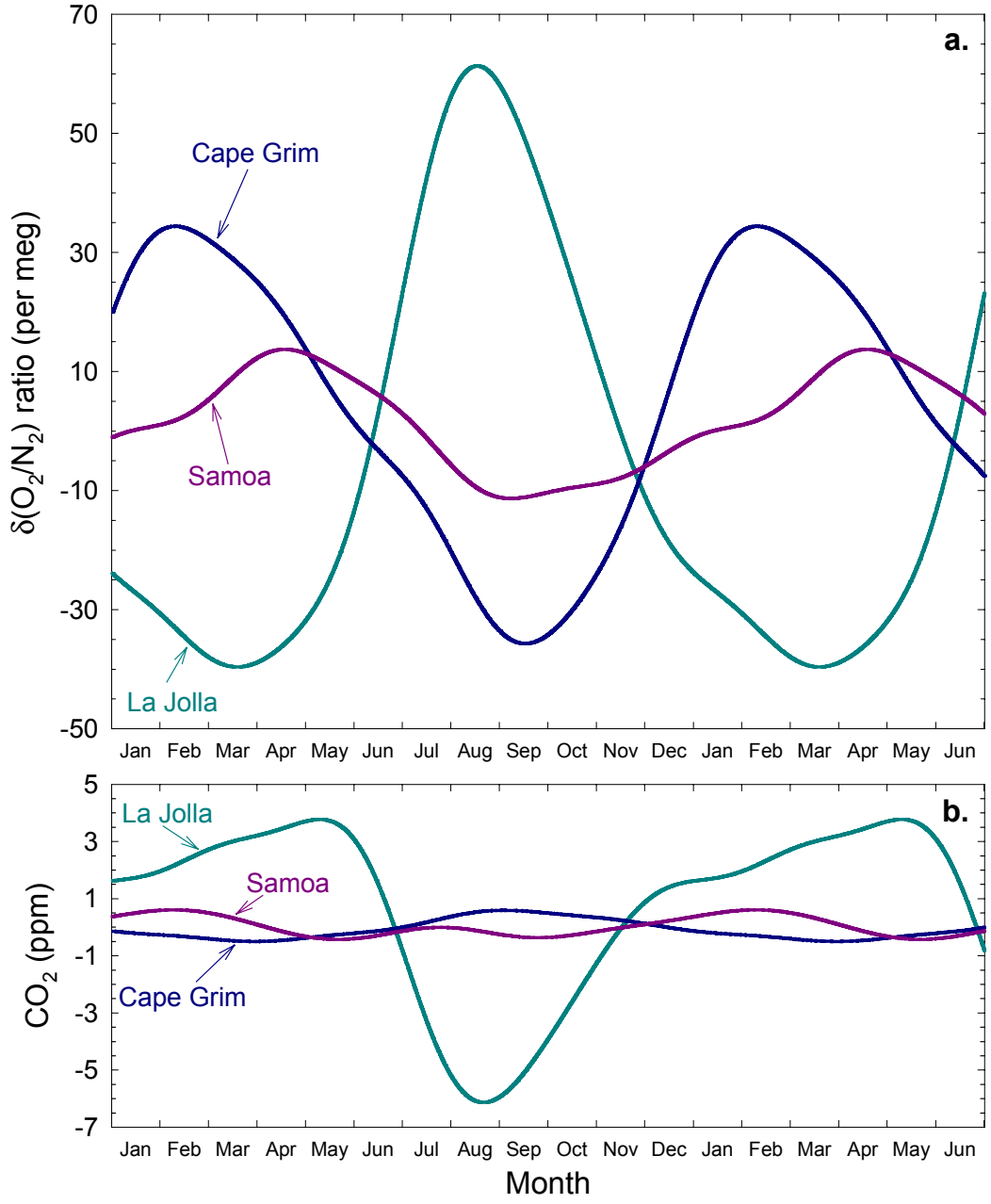

Figure 2.9. Four-harmonic seasonal components of the Samoa curve fits in Figures 2.2 and 2.3, showing O_2/N_2 ratios (a) and CO_2 concentrations (b). Also shown for comparison are similar seasonal curve fits calculated from Cape Grim and La Jolla, representing the mid-latitudes of the southern and northern hemisphere respectively. To show the seasonal characteristics more clearly, the first six months of each cycle are repeated. Southern hemisphere and northern hemisphere cycles are roughly six months out of phase with each other, whereas Samoa shows a more complicated signal. Plots a and b have been scaled so that changes in O_2 and CO_2 can be compared visually on a mole to mole basis.

Samoa, as seen in the figure. The La Jolla curves show that Samoa O_2/N_2 ratios and CO_2 concentrations are also not in phase with northern hemisphere trends. In addition, at each of La Jolla and Cape Grim, O_2/N_2 and CO_2 changes are to a good approximation anti-correlated with each other, whereas at Samoa this is clearly not the case.

The unique climatological conditions at Samoa and their impact on concentrations of atmospheric constituents have been noted before. *Halter et al.* [1988] presented three years of CO_2 data from 1979-1981. They discussed the seasonal dependence of the variability observed in their CO_2 data and related this to air masses arriving at Samoa from different source regions. Following the wind climatology at Samoa presented by *Bortniak* [1981] and from an analysis of wind backward trajectories, *Halter et al.* [1988] were able to show that the air arriving at Samoa came from one of three broadly-defined source regions centered on anticyclones named A_{NP}, A_{SP}, and A_{ANZ}, representing the north Pacific tropical anticyclone, the southeast Pacific tropical anticyclone, and the Australia-New Zealand anticyclone respectively. These source regions are shown in Figure 2.10.

Halter et al. [1988] further demonstrated that the observed Samoa CO_2 seasonal cycle was a superposition of three distinct seasonal cycles originating from each of these three air mass source regions. Because the seasonal cycle of CO_2 in the northern and southern hemispheres are out of phase, these cancel out partially, but not completely, at Samoa, resulting in the complex seasonal pattern which can be seen in Figure 2.9b. Halter *et al.* [1988] then showed that the seasonal dependence of the CO_2 variability observed at Samoa is a function of the seasonally varying interhemispheric gradient in CO_2 concentration, and also of the seasonally varying frequency of occurrence that air

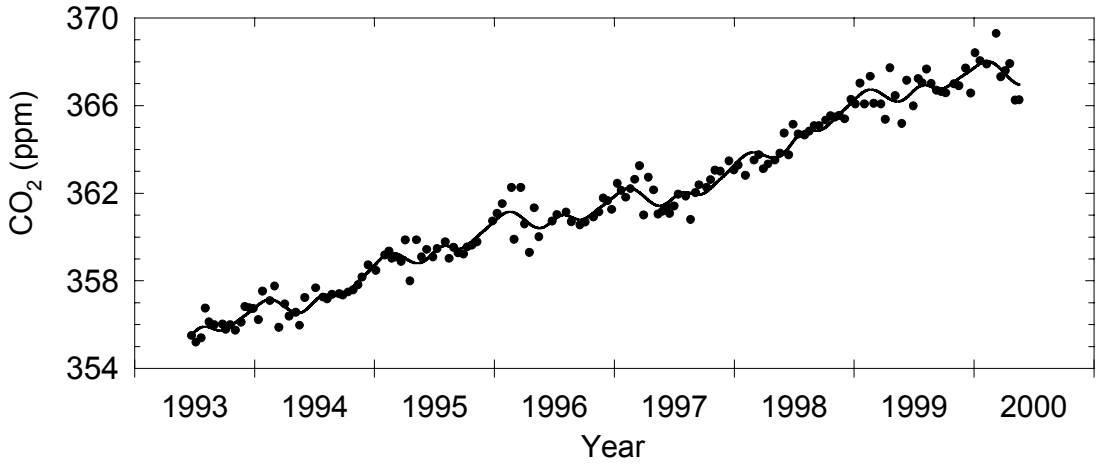

Figure 2.11. Samoa CO_2 data, as shown in Figure 2.3, enlarged here to show the contrast in variability between El Niño and non-El Niño years. During the strong El Niño of 1997-1998 a lack of variability during austral summer can be seen.

2.4.2. Land and Ocean Partitioning of Air Mass Influences at Samoa

In Figure 2.12, I show plots of APO and CO_2 concentrations representing oceanic and land influences at Samoa respectively. The symbols on each plot show all flask samples collected at Samoa from June 1993 to June 2000, where all samples have been collapsed into one calendar year. The curves shown are the four-harmonic seasonal component of the curve fits to data from Cape Grim and Cape Kumukahi, representing the nearest sampling stations from which I have data in the southern and northern hemispheres respectively. Typically, data that have been interannually detrended are centered on zero and have no absolute frame of reference. Here, in order to compare detrended data across different stations, I have normalized all data to the Cape Grim interannual trend. In other words, the Samoa flask data shown are the raw data points from the Samoa plots of Figures 2.4 and 2.3 with the interannual spline component of the Cape Grim curve fit subtracted. Because of slight variability from

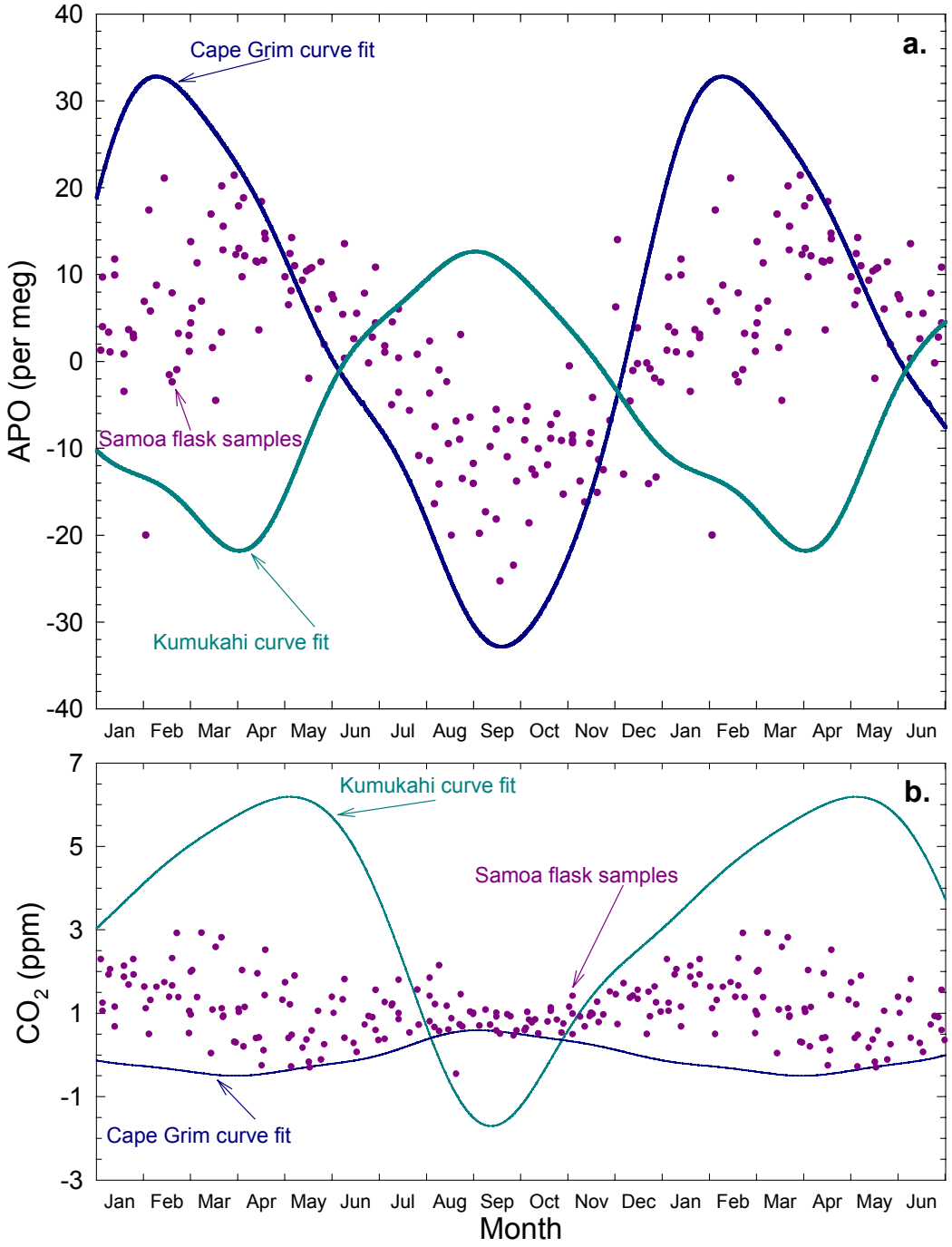

Figure 2.12. Shows oceanic (a) and land biotic (b) influences on the air masses arriving at Samoa. Atmospheric Potential Oxygen (APO), defined in the text (section 2.2.2), is essentially not influenced by land biotic processes and therefore represents oceanic influences. The seasonal component of the Samoa flask samples are shown, as well as seasonal curve fits from Cape Grim and Cape Kumukahi, representing the nearest stations from which I have data in the southern and northern hemisphere respectively. Data have been normalized as described in the text. As with Figure 2.9, the first six months of each cycle are repeated, and the plots have been scaled to be able to visually compare mole to mole changes in APO and CO_2 concentrations.

year to year in the interannual trends, I am not able to show the Kumukahi four-harmonic curve fit in the same manner. Instead, I calculated the average offset between the Kumukahi and Cape Grim spline components from 1993 to 2000 ($\Delta O_2/N_2$ = -3.6 per meg; ΔCO_2 = 2.8 ppm) and added this offset to the Kumukahi four-harmonic curve fit, resulting in the Kumukahi curves shown in Figures 2.12a and b. The Cape Grim curves shown are simply the Cape Grim four-harmonic components of the Cape Grim curve fits. As with Figure 2.9, the first six months are repeated to generate 18 months of data, and APO and CO_2 changes are comparable visually on a mole to mole basis.

There are several prominent features apparent in Figure 2.12. Samoa CO_2 data in Figure 2.12b agree very well with the earlier data presented by *Halter et al.* [1988], showing greater variability in the austral summer and autumn. However, based on additional information from our APO data, I suggest a slightly different hypothesis of source air mass origins to explain this variability. For periods of May, June, and December in the APO signal, and from August to October in the CO_2 signal, Samoa data exhibit persistently higher concentrations than seen in air masses either to the north or to the south. I believe that these data represent recirculated air, perhaps as a component of the Pacific Walker cell circulation, in other words air not recently originating from the north or the south, but from the tropics at some point in the past.

To further support this hypothesis, in Figure 2.13 I present the statistical variability in the data. I calculated the residuals of all Samoa flask samples from the plots in Figures 2.4 and 2.3 from the curve fits also shown in the Samoa plots of Figure 2.4 and 2.3. I then calculated the standard deviation of these residuals for each month, where, for example, all January samples from 1993 to 2000 have been binned together.

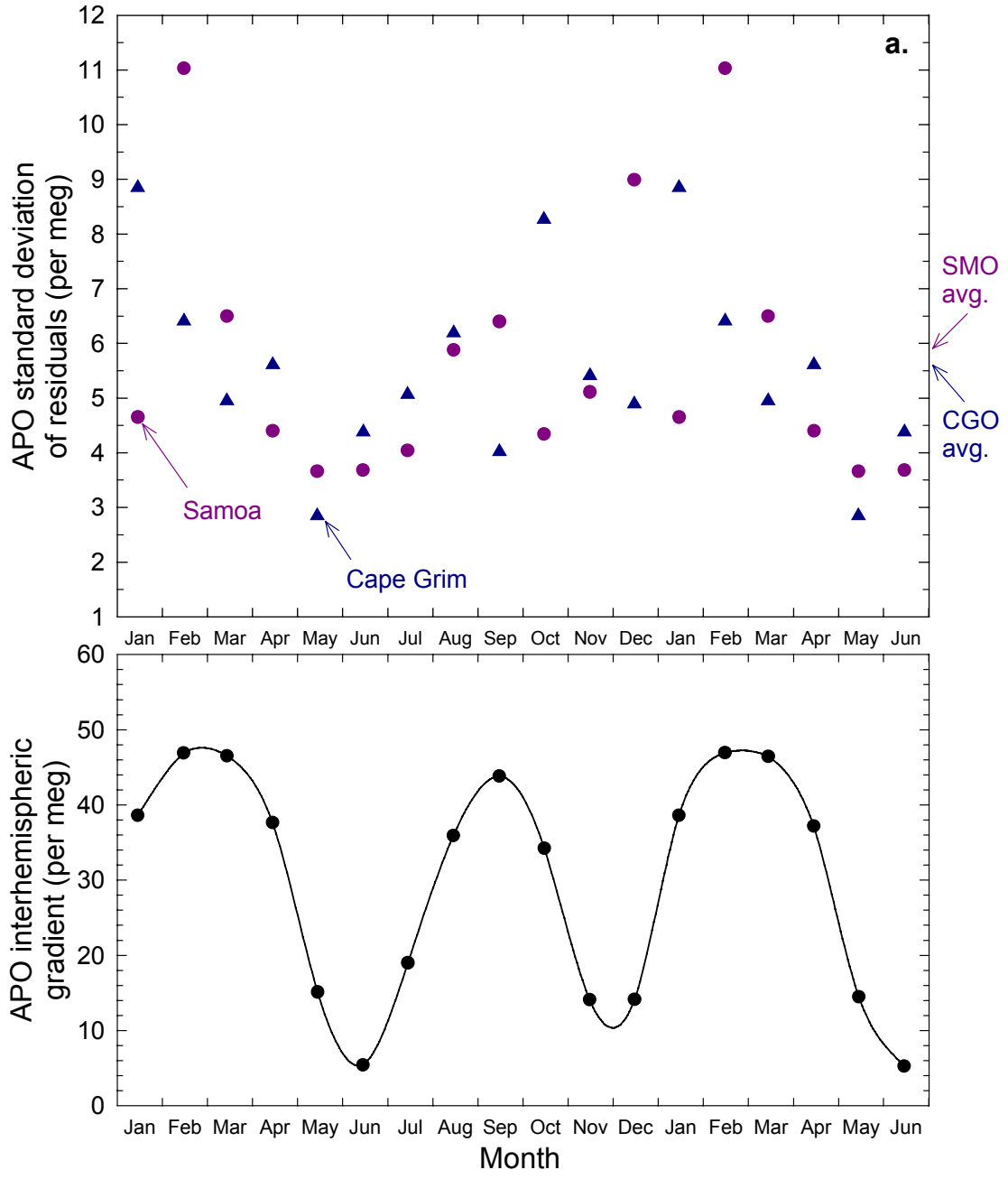

Figure 2.13a. The top plot shows APO monthly standard deviations of the residuals of the flask data from Figure 2.4 from the curve fits in the same figure. Results are shown for both Samoa and Cape Grim, and the first six months are repeated. The annual average residual at each station is indicated on the right. There is little to distinguish between Samoa and Cape Grim, and there is only weak evidence of a seasonal trend in the residuals at both stations. The bottom plot shows the absolute magnitude of the north-south interhemispheric gradient, calculated each month, and using Cape Grim and Cape Kumukahi data as representative of the southern and northern hemisphere respectively to calculate the gradient.

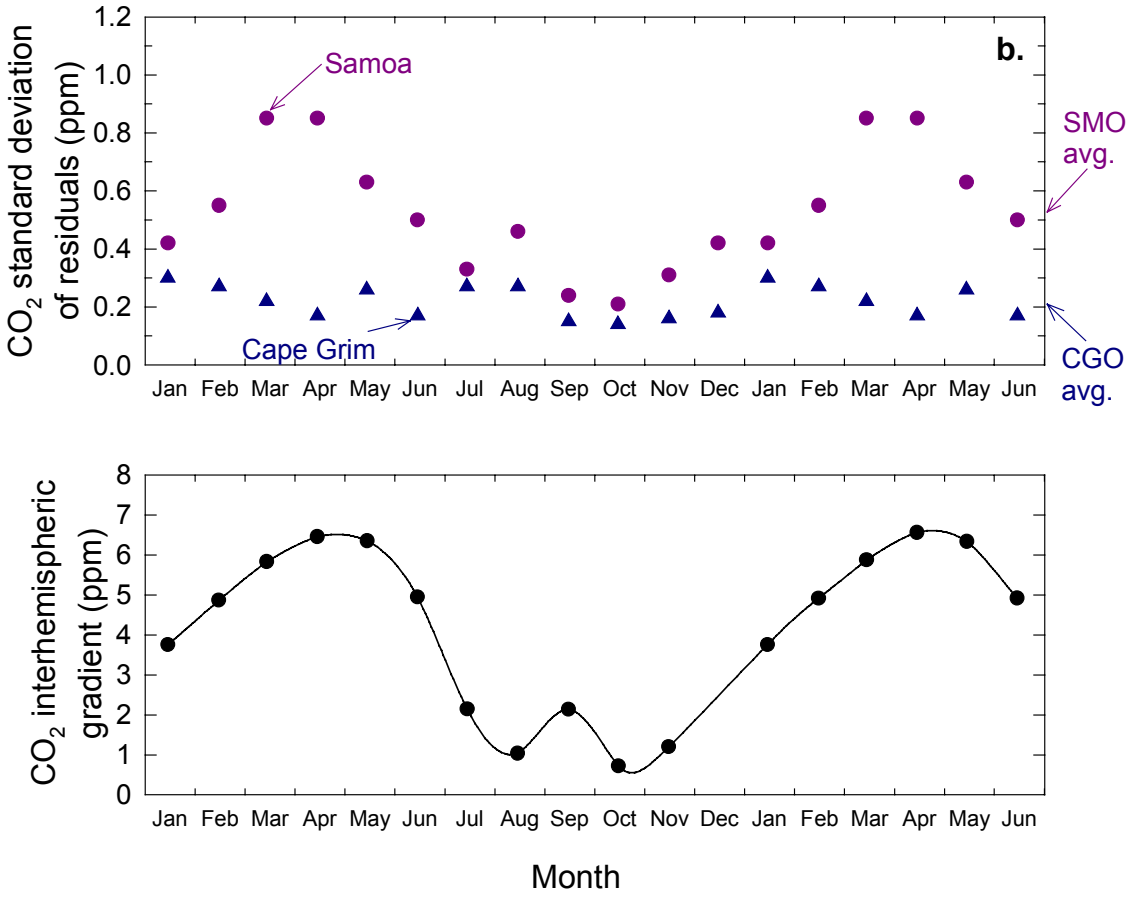

Figure 2.13b. Top and bottom plots as for Figure 2.13a, except showing CO_2 concentration. As for Figures 2.9 and 2.12, APO and CO_2 changes are visually comparable between Figures 2.13a and b. In contrast to APO, CO_2 shows a clear seasonal pattern in variability at Samoa, indicated here with higher standard deviations, whereas Cape Grim does not appear to show any seasonality. The pattern at Samoa appears to correlate well with the north-south interhemispheric gradient. Contrasting the magnitude of APO variability with CO_2, it can be seen that the APO signal is much "noisier", reflecting the presence of larger sources and sinks for O_2 in the southern hemisphere compared to CO_2.

These standard deviations for each month are shown in the top plots of Figures 2.13a and 2.13b for APO and CO_2 respectively. Thus these plots give a statistical measure of the variability in APO and CO_2 at monthly time intervals. To provide a comparison,

Cape Grim data are calculated in the same manner. As for Figures 2.9 and 2.12, the first six months are repeated.

Figure 2.13b shows what was readily apparent in Figure 2.12b, a clear seasonal pattern to the variability in the CO_2 signal. The figure also shows a good correlation of this variability with the north-south interhemispheric gradient, shown in the bottom plot of Figure 2.13b. In contrast, the top plot of Figure 2.13b shows that Cape Grim does not exhibit such seasonal variability, and that during the austral winter and spring, Samoa variability is similar to that at Cape Grim. Figure 2.13a shows that there may also be a seasonal component to the APO variability. However, such seasonality is much less readily apparent than the CO_2 seasonality, is not of the same phasing as CO_2, and is almost equally apparent in Cape Grim APO as it is in Samoa APO.

With the exception of APO in December, all of the months described above in Figure 2.12 exhibiting APO or CO_2 concentrations higher than present in the northern or southern hemisphere for that month also show relatively low monthly standard deviations in Figure 2.13. This lower variability also suggests that this air has had more time to mix and become homogenized, and has not been influenced to the same extent by air masses from the north or the south, supporting the hypothesis of recirculated tropical air.

Figures 2.12 and 2.13 both show a clear difference in the pattern of variability in the APO signal compared with the CO_2 signal. APO does not show such a clear seasonal distinction in variability as CO_2, and does not show significant differences from Cape Grim variability (Figure 2.13). The top plots of Figure 2.13 have been scaled to enable direct comparison of the magnitude of variability of APO with CO_2. Thus it is

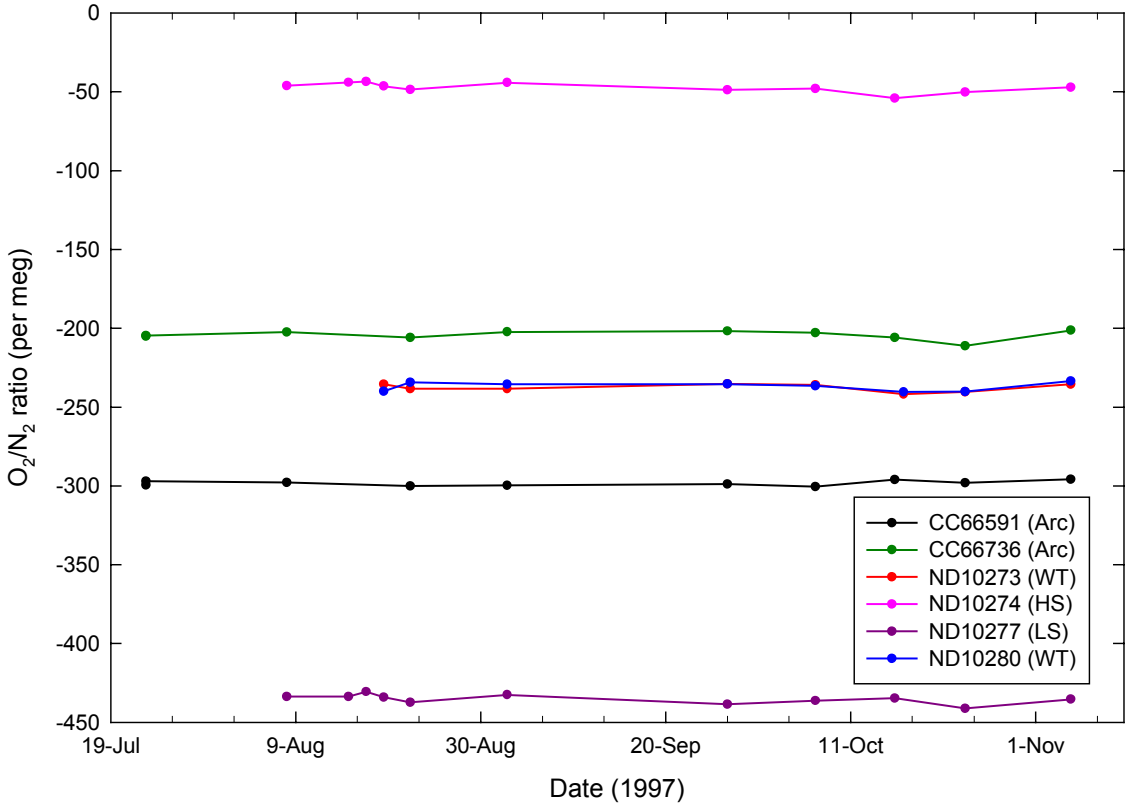

Figure 4.5. Shows the O_2/N_2 ratios calculated on the interferometric analyzer at Scripps of the calibration gases used at Baring Head. "Arc" indicates long-term archive gas cylinders, "WT" indicates working gases, and "HS" and "LS" are high span and low span gases respectively. All gases show good stability in O_2/N_2 ratios over a three to four month period.

(Table 4.1), I can then calculate a daily value for the O_2/N_2 ratio of the working gas. I assign this value for the next 24 hours, until the next HS/LS calibration runs and re-calculates the working gas ratio. Figure 4.6 shows the results of these calculations. Five different working gases have been used in the first 12 months of operation, and these are shown labeled above the data in the figure. Small downward trends are apparent in the working gas concentrations over time. This is probably demonstrating a real change in O_2/N_2 ratio in the cylinders and is most likely owing to decreasing

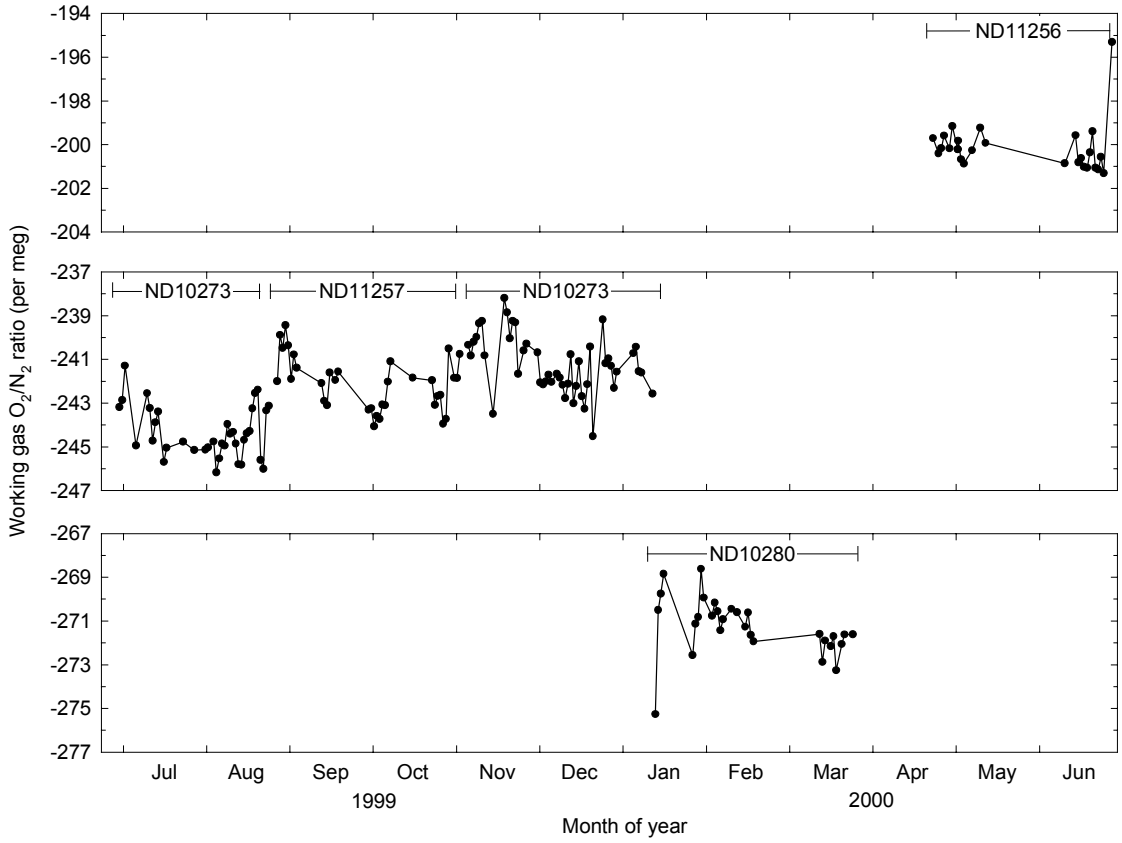

Figure 4.6. Working gas O_2/N_2 ratios as calculated from daily calibrations of the working gas against the high span and low span cylinders. Five different working gases have been used in the first year of operation at Baring Head, as labelled in the figure. Each panel shows a 10 per meg range, showing that the working gases are very stable over their lifetime.

cylinder pressure resulting in desorption from the tank walls, as discussed in *Keeling et al.* [1998]. Standard deviations of each working gas over its lifetime range between ±1.2 and ±1.3 per meg, with between 30 and 50 total daily calibration analyses. Several gaps can be seen in the record of Figure 4.6. These are because of 'bad' calibrations, or analyzer down-time. Continuous atmospheric O_2 measurements are in their infancy, and technical and programming problems continue to arise. With the very limited personnel support that NIWA was able to provide, only travelling to the station once

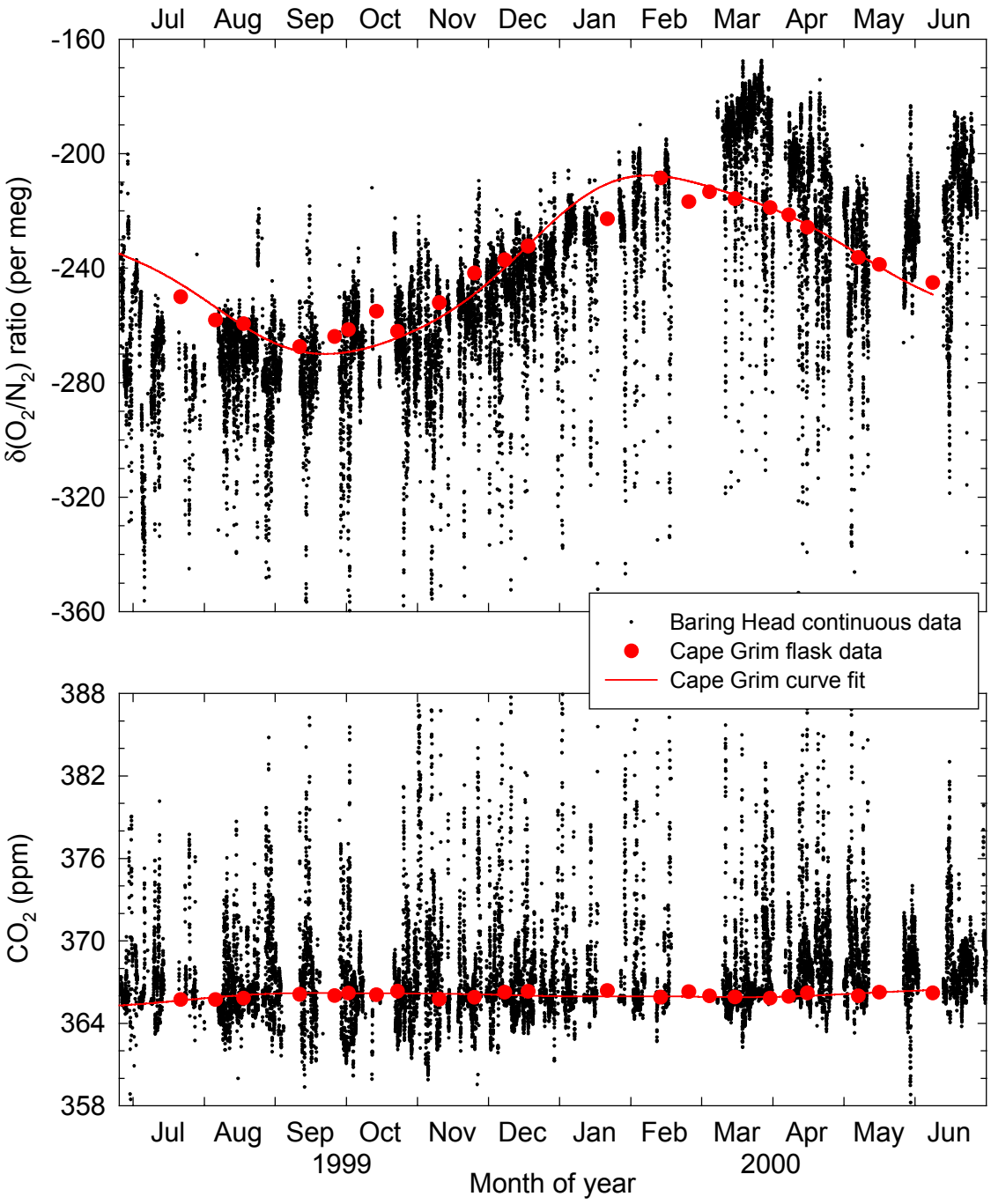

Figure 4.9. Shows all O_2/N_2 ratio and CO_2 concentration data collected at Baring Head from June 1999 to July 2000. Each black data point is an average over 15 minutes. Red data points show flask samples collected at Cape Grim, Tasmania (see Figure 4.1) during clean, background air conditions as a part of the Scripps O_2/N_2 flask sampling network. The red line is a curve fit to the Cape Grim data.

A clear seasonal cycle can be seen in O_2/N_2 ratios with a minimum occurring at the end of winter, in late August or early September, and a maximum occurring in late March, at the end of summer. No seasonal cycle is apparent in the CO_2 data, at least not at the scale shown in Figure 4.9b. This suggests that almost all of the seasonal cycle in O_2/N_2 can be explained by oceanic processes, and this is confirmed in Figure 4.10 which shows the oceanic-only influence on the O_2/N_2 ratios, as defined by Atmospheric Potential Oxygen (APO, see section 2.2.2. for a definition) showing a similar amplitude in the seasonal cycle of APO as in O_2/N_2 ratios. O_2/N_2 ratios (and APO) increase in spring and summer because of increased photosynthetic activity in the oceans producing dissolved O_2, and because of shoaling of the mixed layer of the ocean which acts to concentrate this O_2 in the surface waters, supersaturating these waters, and driving a net flux of O_2 into the atmosphere. In addition, warming of the surface ocean in the spring and summer reduces the solubility of the water, causing further O_2 supersaturation and adding to the O_2 flux to the atmosphere. This activity peaks in March, then biological activity decreases producing less O_2, the surface ocean cools becoming more soluble, and the mixed layer deepens, incorporating O_2-depleted waters into the surface layer. These processes all act together to produce a net demand of O_2 to the atmosphere and the O_2/N_2 ratio (and APO) is observed to decrease.

Whereas O_2/N_2 ratio and CO_2 concentration data display asymmetric patterns, with O_2/N_2 ratio scatter falling below the baseline and CO_2 concentration scatter occurring above the baseline, APO data in Figure 4.10 shows more symmetric scatter, and less overall scatter to the data. This observation further demonstrates that for the most part, O_2/N_2 ratios and CO_2 concentrations are anti-correlated.

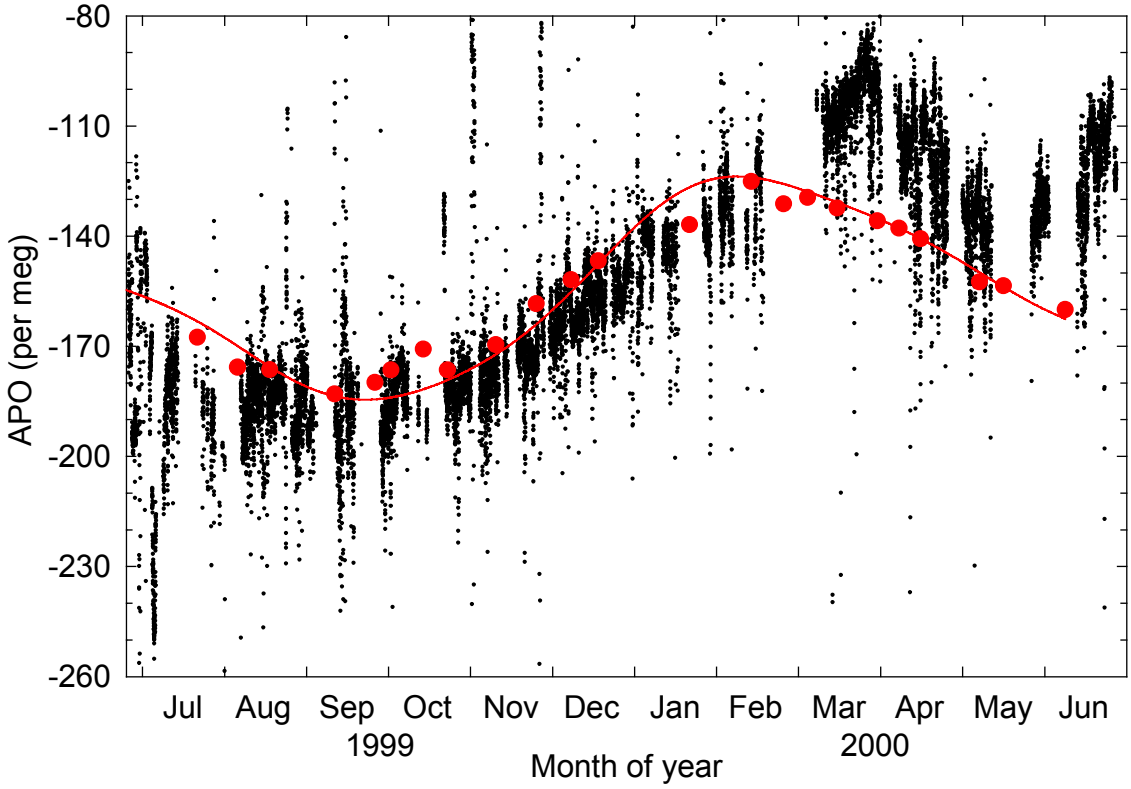

Figure 4.10. Atmospheric Potential Oxygen, APO, at Baring Head from June 1999 to July 2000. This shows the oceanic influence on the air arriving at Baring Head.

Also shown in Figures 4.9 and 4.10, as red symbols, are flasks samples collected at Cape Grim, Tasmania (40.7°S, 144.7°E) as part of our global flask sampling network (Chapter 2). These flask samples are shipped back to our laboratory in La Jolla, California, where they are analyzed for O_2/N_2 ratio on our interferometric analyzer [*Keeling*, 1988] and for CO_2 concentration on a Siemens NDIR analyzer. Curve fits to the Cape Grim data are also shown, consisting of the sum of a four-harmonic seasonal cycle and a stiff spline. The curve fits were calculated from a longer dataset not shown, extending back to 1991.

Cape Grim flask samples are collected only when meteorological conditions are such that the air sampled is thought to be representative of a large, regional area of the mid-latitudes of the southern hemisphere, not influenced by local or regional anthropogenic or land biotic processes. Therefore, because Cape Grim is at a similar latitude as Baring Head, I can expect reasonable agreement between the two stations, when Baring Head data are also not influenced by these processes. Therefore, in general, I would expect the high O_2/N_2 ratios and low CO_2 concentrations from Baring Head to show reasonable agreement with the Cape Grim data. As illustrated in Figure 4.9a, such agreement for O_2/N_2 ratios is true from July 1999 to February 2000. In March 2000 the Baring Head trend departed significantly from the Cape Grim trend, showing O_2/N_2 ratios elevated by as much as 40 per meg. A similar trend is seen in the comparison of the APO data. From the CO_2 data in Figure 4.9b, it is difficult to determine if Baring Head and Cape Grim records are in agreement.

To investigate the comparison between the two stations in greater detail I have filtered the Baring Head data to only retain data collected under southerly wind conditions, when the local wind direction was between 135° and 225°, and when the local wind speed was greater than 20 km/h. For the most part, these data will be uninfluenced by anthropogenic or land biotic processes, representing air masses recently originating from the Southern Ocean, and thus comparable to Cape Grim flask data. Figure 4.11 shows these filtered data for O_2/N_2 ratios and CO_2 concentrations, and Figure 4.12 shows APO filtered data. Both figures include the same Cape Grim data and curves.

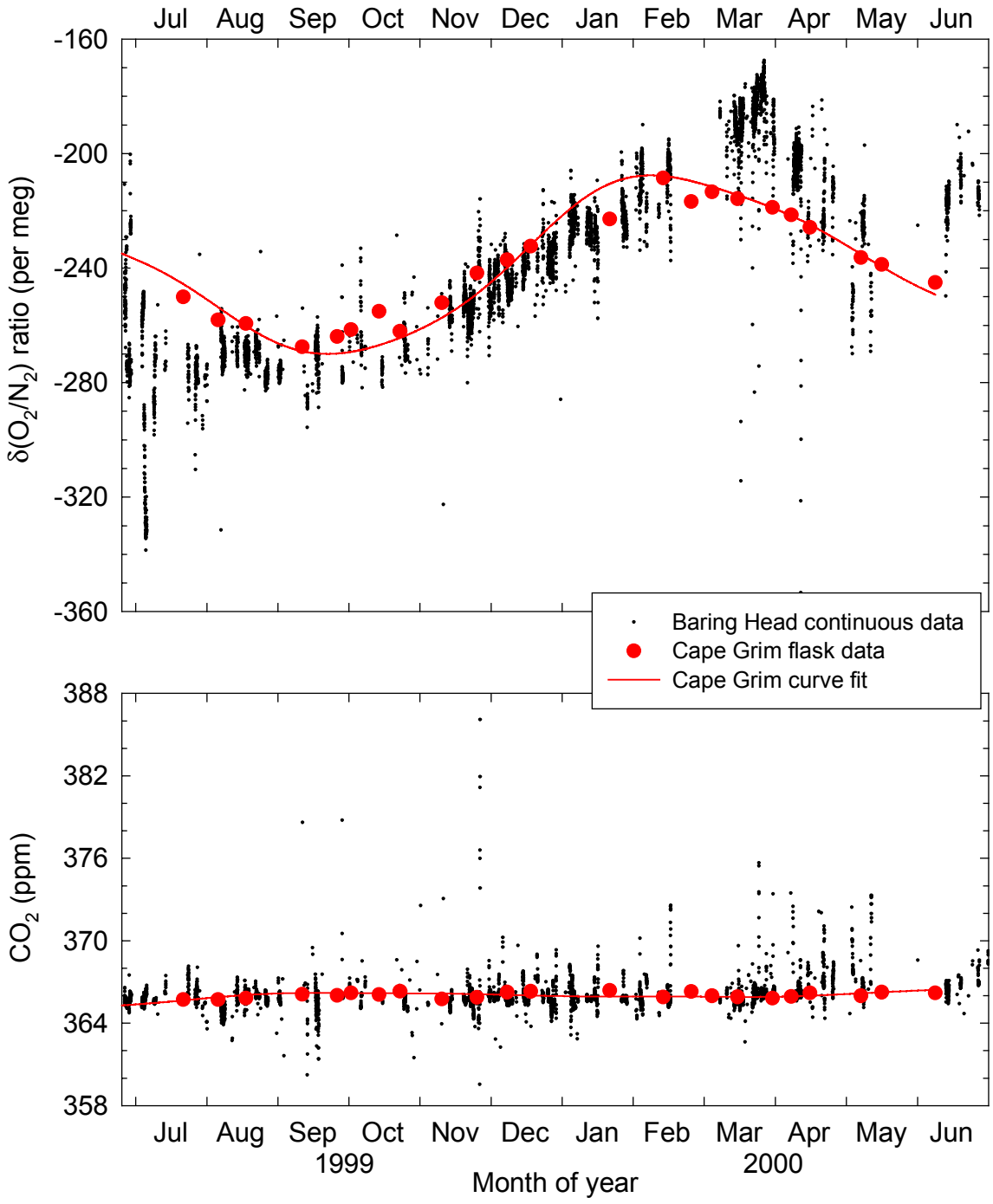

Figure 4.11. As for Figure 4.9, except data have now been filtered to only show data when conditions are thought to be representative of clean, background air. That is, the wind direction is between 135° and 225°, and the wind speed is greater than 20 km/h.

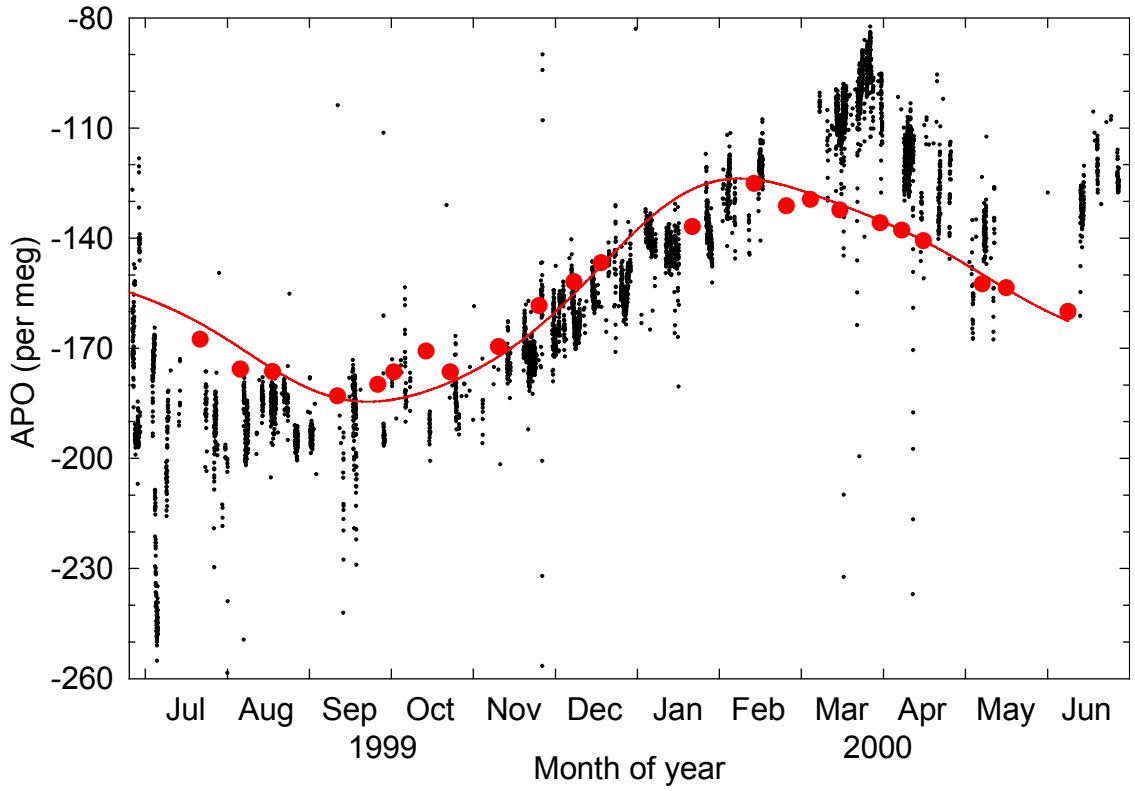

Figure 4.12. As for Figure 4.10, except data have now been filtered to only show data when conditions are thought to be representative of clean, background air, as in Figure 4.11. That is, the wind direction is between 135° and 225° and the wind speed is greater than 20 km/h.

Baring Head CO_2 data now show reasonably good agreement with Cape Grim for the one year record. O_2/N_2 ratio and APO data still show the same prominent differences observed in Figures 4.9a and 4.10. Ignoring for the moment data in June 2000, the March, April, and May 2000 data appear to indicate a later summertime O_2/N_2 (and APO) peak at Baring Head than Cape Grim and a subsequent faster drawdown of O_2/N_2 (and APO) in autumn. In addition, at the beginning of the record, in June and July 1999, there is tentative evidence for an earlier wintertime minimum in O_2/N_2 ratio

checked to ensure that there was no evidence of instrumental or calibration anomalies for the duration of this event.

As shown in Figure 4.14, O_2/N_2 was initially relatively constant, and about 15 per meg lower than expected when compared to results from our flask sampling program at Cape Grim. Then O_2/N_2 was observed to decrease in an approximately linear fashion over a period of approximately 18 hours by 80 per meg. Finally, the O_2/N_2 ratio steadied at a very low value of about –330 per meg, then the baseline event ended dramatically as the wind changed, and O_2/N_2 decreased further, before recovering again. In this latter case changes are clearly due to anthropogenic or land biotic sources and sinks. Unfortunately, at the beginning of the dramatic decrease in O_2/N_2 ratios at about 12:00, 4 July, there is a 2.5-hour gap in the data when the O_2 analyzer carried out a daily calibration cycle. Despite this missing data, I am confident that the existing data support the conclusion that a downward trend in O_2/N_2 began at about the same time that the calibration started. A second gap seen in the data at the same time on 5 July is the following day's calibration.

Also shown in Figure 4.14 is the CO_2 concentration over the same time period and on the same effective scale so that molar changes are comparable for both O_2 and CO_2 on a visual basis. Note that the CO_2 concentration scale has been reversed so that decreases in O_2/N_2 will have the same sign as increases in CO_2 concentration. These data appear to show that CO_2 was relatively constant over this time period, which is what one would generally expect during a baseline event. However, when I expand the CO_2 scale, as shown in Figure 4.15, a relatively significant increase in CO_2 of at least 1.5 ppm is observed. Unfortunately the Baring Head CO_2 analyzer was experiencing

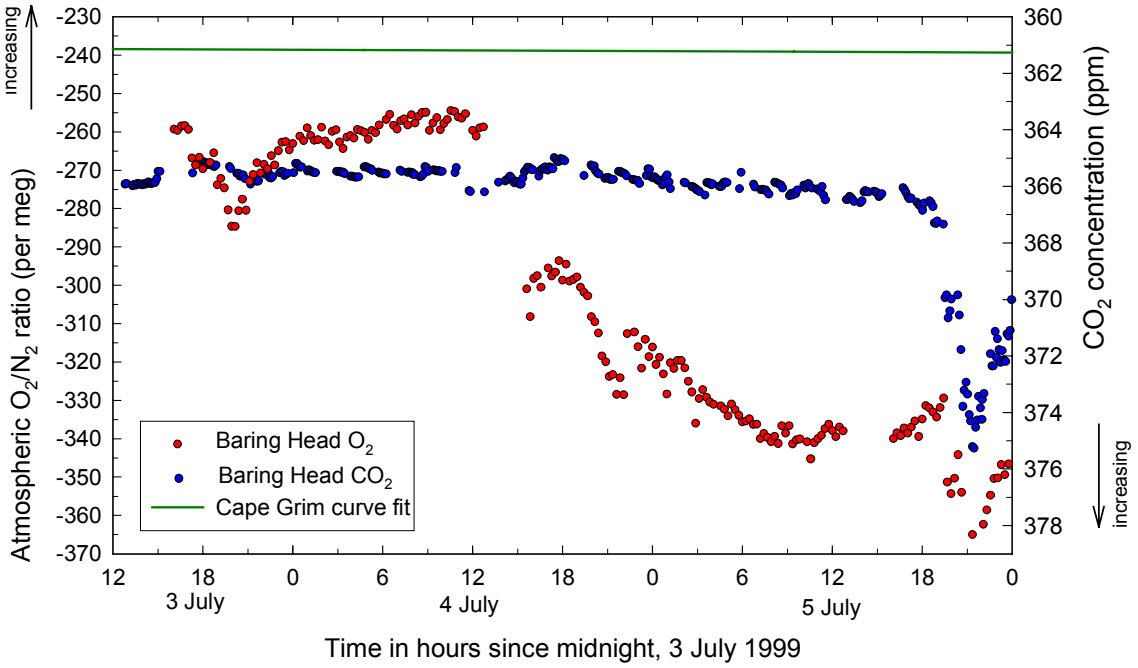

Figure 4.14. O_2/N_2 ratio and CO_2 concentration at Baring Head for 3-5 July 1999. Note that O_2/N_2 ratio and CO_2 concentration axes are reversed with respect to each other. In addition these axes are scaled so that changes in O_2 and CO_2 are comparable on a mole to mole basis. The green line shows the curve fit to the O_2/N_2 ratio data from flask samples collected at Cape Grim, Tasmania.

some technical problems during this time period, as illustrated by the abnormally noisy signal. Therefore a more precise determination on the exact increase in CO_2 concentration can not be made, however, it is clearly of the order of 1.5 ppm.

These changes in O_2/N_2 ratio and CO_2 concentration can not be attributed to land biotic or anthropogenic effects, because the observed O_2:C molar ratio is approximately –11:1, instead of –1.1:1 that would be observed from land biotic effects, or –1.4:1 that would be observed from fossil fuel combustion. This leaves only oceanic processes that could be responsible for the observations.

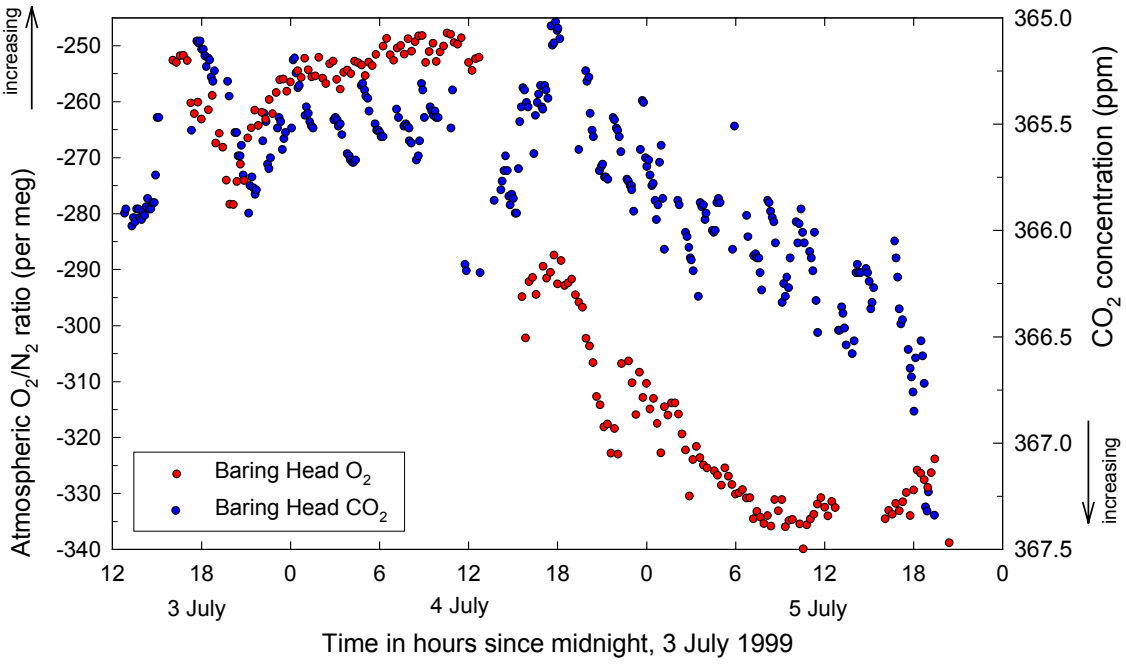

Figure 4.15. As for Figure 4.14, except the CO_2 axis has been blown up, showing that CO_2 concentrations increased at the same time that O_2/N_2 ratios decreased.

To help identify the origin of the sampled air, I have calculated 72-hour backward wind trajectories using the HYbrid Single-Particle Lagrangian Integrated Trajectory model, version 4 (HYSPLIT4), developed by the NOAA Air Resources Laboratory [*Draxler and Hess*, 1998]. This model uses 1° meteorological analyses from the National Center for Environmental Prediction as input fields. In Figure 4.16, I show one such trajectory calculation for air arriving at Baring Head at 12:00, 4 July 1999 NZST. This figure clearly shows that the air arriving at Baring Head was solely of oceanic origin, and from relatively high latitudes in the Southern Ocean.

There is some concern regarding the accuracy of such trajectory models in the southern hemisphere where direct observations are relatively sparse and the model must

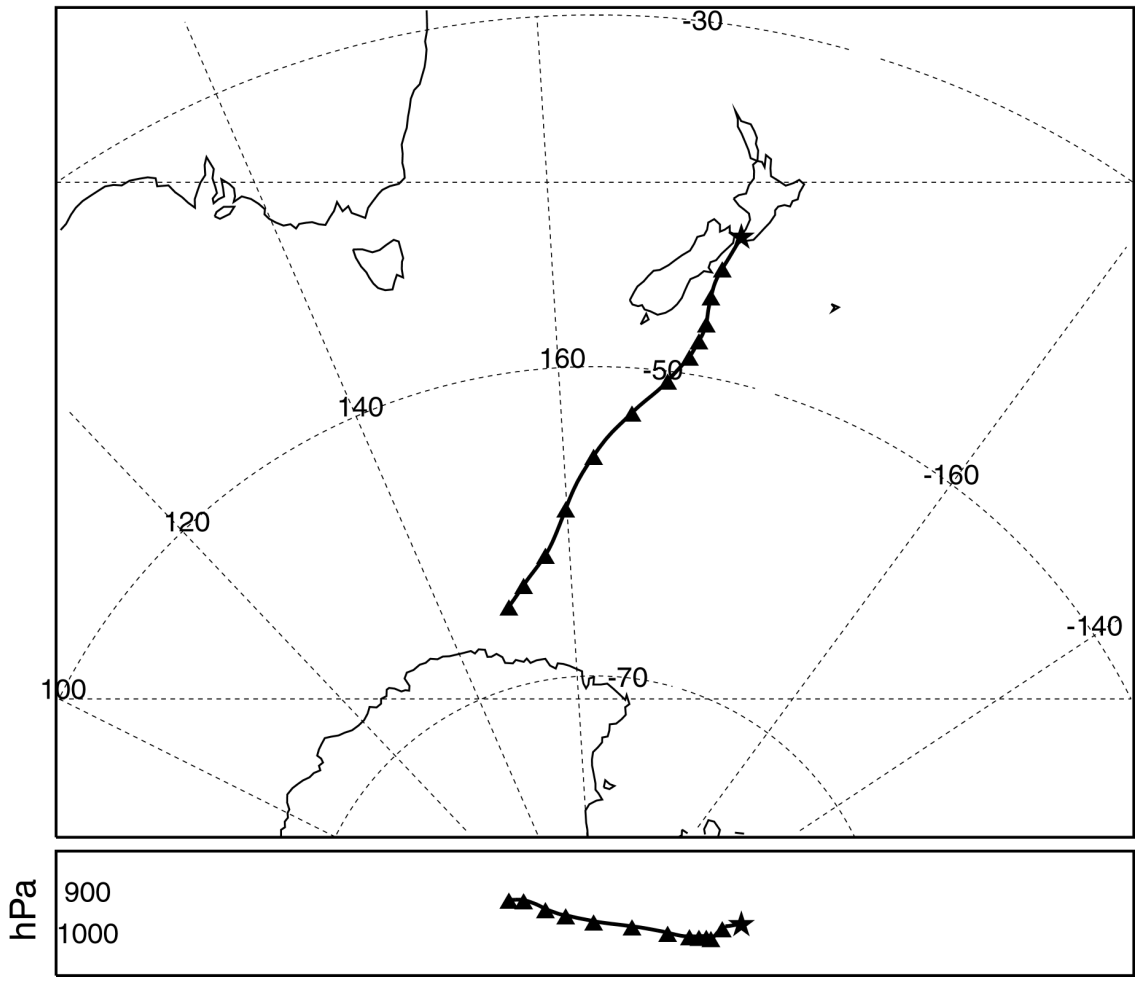

Figure 4.16. Three-day backward wind trajectory ending at 12:00 4 July 1999 at Baring Head, New Zealand. Calculated using the HYSPLIT program (see text). This shows that during this southerly event, wind was derived from high latitudes in the Southern Ocean and has not passed over any land mass, in particular missing the South Island of New Zealand.

rely heavily on satellite scatterometer winds and interpolation routines. Therefore I calculated back trajectories at many other times not shown here, including at the start and end of the baseline event, as indicated by the observed wind changes at Baring Head. The HYSPLIT model captured all of these observed wind changes remarkably